On synchronous supereruptions

Alejandro Cisneros de León[1], Tushar Mittal[2], Shanaka L. de Silva[3], Stephen Self[4], Axel K. Schmitt[1], and Steffen Kutterolf[5]

[1]Heidelberg University
[2]Massachusetts Institute of Technology
[3]Oregon State University
[4]University of California
[5]GEOMAR Helmholtz Centre for Ocean Research

November 21, 2022

Abstract

Two recent supereruptions (magnitude (M) scale [?] 8), the Young Toba Tuff (YTT), Sumatra, and the Los Chocoyos (LCY), Guatemala, are found to be statistically synchronous at ca. 74 ka and near antipodal. Such planetwide synchroneity of supereruptions is shown to be statistically non-random implying a causal link. We propose that the seismic energy release from the YTT supereruption may have initiated eruption from the contemporaneous "perched" LCY magma system. This near-equatorial supereruption "double-whammy" may be the more compelling source of the significant environmental impacts often attributed to a singular YTT eruption.

On synchronous supereruptions

A. Cisneros de León[1]*†, T. Mittal[2]*†, S.L. de Silva[3], S. Self [4], A.K. Schmitt[1], S. Kutterolf [5]

[1]Institute of Earth Sciences, Heidelberg University; Heidelberg, Germany.
[2]Department of Earth, Atmosphere and Planetary Sciences, Massachusetts Institute of Technology; Cambridge, USA.
[3]College of Earth, Ocean, and Atmospheric Sciences, Oregon State University; Corvallis, USA.
[4]Earth and Planetary Science Department, University of California; Berkeley, USA.
[5]GEOMAR Helmholtz Centre for Ocean Research; Kiel, Germany.

*Corresponding author. Email: cisneros.deleon@outlook.de

†These authors contributed equally to this work.

Abstract

Two recent supereruptions (magnitude (M) scale ≥ 8), the Young Toba Tuff (YTT), Sumatra, and the Los Chocoyos (LCY), Guatemala, are found to be statistically synchronous at ca. 74 ka and near antipodal. Such planetwide synchroneity of supereruptions is shown to be statistically non-random implying a causal link. We propose that the seismic energy release from the YTT supereruption may have initiated eruption from the contemporaneous "perched" LCY magma system. This near-equatorial supereruption "double-whammy" may be the more compelling source of the significant environmental impacts often attributed to a singular YTT eruption.

Keywords: Young Toba Tuff, Los Chocoyos, Climate Change

Introduction

Catastrophic caldera-forming supereruptions are next to the impact of kilometer-sized bolides, the most intense events affecting the Earth system. These low-frequency but high-intensity volcanic "Black Swans" are capable of explosively ejecting ≥1000 km^3 of high-silica tephra at geologically instantaneous timescales (magnitude (M) scale ≥ 8) (Pyle, 2015). The recorded and expected impacts of such supereruptions range from local to global in scale: complete devastation up to hundreds of kilometers away from the eruptive vent by ground-hugging hot and turbulent pyroclastic density currents (Roche et al., 2016) and regional-scale economic, social, and eco-system disruption by tephra fall (Miller and Wark, 2008), that may extend to the global scale over several years to decades through the release of significant amounts of climate-forcing gases such as sulfur, chlorine, and bromine (Brenna et al., 2020; Brenna et al., 2021; Self, 2015).

In the last 2 Myr, at least 13 supereruptions have occurred globally (Crosweller et al., 2012) with an estimated recurrence interval of *ca*. 150 kyr, a timescale shorter than the frequency of meteorite impacts (*ca*. 0.6-3 Myr)(Bland, 2005) large enough to potentially have similar environmental consequences (Rampino, 2002). If the eruption record of only the last *ca*. 100 kyr is considered, the recurrence interval further decreases to *ca*. 17 kyr (Rougier et al., 2018). Given the likelihood that established eruption databases are incomplete (Crosweller et al., 2012) these rates could be considered maxima and a temporal coincidence of supereruptions is not *a priori* unlikely. Synchronous, paired, or grouped, large (M7 to M8) eruptions have been proposed within various volcanic regions (e.g., de Silva et al., 2006; Gravley et al., 2007), but synchroneity of eruptions ≥M8 on a global scale is hitherto unknown. The discovery of two apparently synchronous recent supereruptions, the *ca*. 74 ka Young Toba Tuff (YTT), Sumatra, and Los Chocoyos (LCY), Guatemala, has implications for the global record of supereruptions and warrants an evaluation of the randomness of paired eruptions at the colossal scale.

Constraints on the timing of YTT and LCY supereruption

Until recently, only three supereruptions had been recognized in the last *ca*. 100 kyr (Crosweller et al., 2012). Among these the YTT event stands out as the largest supereruption in the Quaternary period, discharging more than 8,600 km^3 tephra (M9.1; Costa et al., 2014) with fallout deposition over an area of ~40 million km^2 (Fig. 1a). The potential release of significant amounts of sulfur gases during this eruption has been putatively linked to a major global climatic downturn reflected in the oxygen isotope record of the Greenland ice cores between

Greenland interstadial 20 and stadial 20 that may have challenged the survival of modern humans (Ambrose, 1998; Rampino and Self, 1992) (Fig. 1b). This hypothesis has been debated due to uncertainties about total sulfur released during the eruption (Oppenheimer, 2002; Robock et al., 2009), the relatively low-precision of existing radioisotopic ages, and YTT volcanic glass shards remaining elusive in ice core records (Abbott et al., 2012; Svensson et al., 2013). However, recent work is tilting the evidence towards a significant environmental impact associated with a solar ultraviolet radiation catastrophe from extreme ozone depletion after the YTT supereruption (Osipov et al., 2021).

Because glass shards of the YTT have not been identified in northern and southern hemisphere ice core archives, the exact SO_4^{2-} spike related to YTT remains ambiguous (Oppenheimer, 2002; Robock et al., 2009; Williams, 2012). Nevertheless, prominent sulfate anomalies occurring in both north and south pole ice-core records have been correlated with YTT (e.g., T2 sulfate spike, Fig. 1b and Fig. S1). However, eight other significant volcanic-derived sulfate anomalies from unknown sources (T1-T9; Fig. 1b and Fig. S1) occur within the uncertainty of the currently accepted radioisotopically determined eruption ages for YTT between 73.9 ± 0.3 ka BP (1σ; $^{40}Ar/^{39}Ar$ in sanidine)(Storey et al., 2012) and 75.0 ± 0.9 ka BP (1σ; $^{40}Ar/^{39}Ar$ in biotite)(Mark et al., 2014) and also indicate large, tropical eruptions (Svensson et al., 2013).

We draw attention to recent work that connotes that the LCY supereruption from the Atitlán caldera in Guatemala, the most recent one from a volcano in the western hemisphere (Cisneros de León et al., 2021), is a potential source for one of these significant sulfate spikes. The age of the LCY was initially estimated from $\delta^{18}O$ stratigraphy at 84 ± 5 ka BP (Drexler et al., 1980) and remained radioisotopically untested for several decades. Recent dating applying (U-Th)/He zircon double-dating has produced a radioisotopic age for LCY of 74.8 ± 1.8 ka BP (1σ) (Cisneros de León et al., 2021).

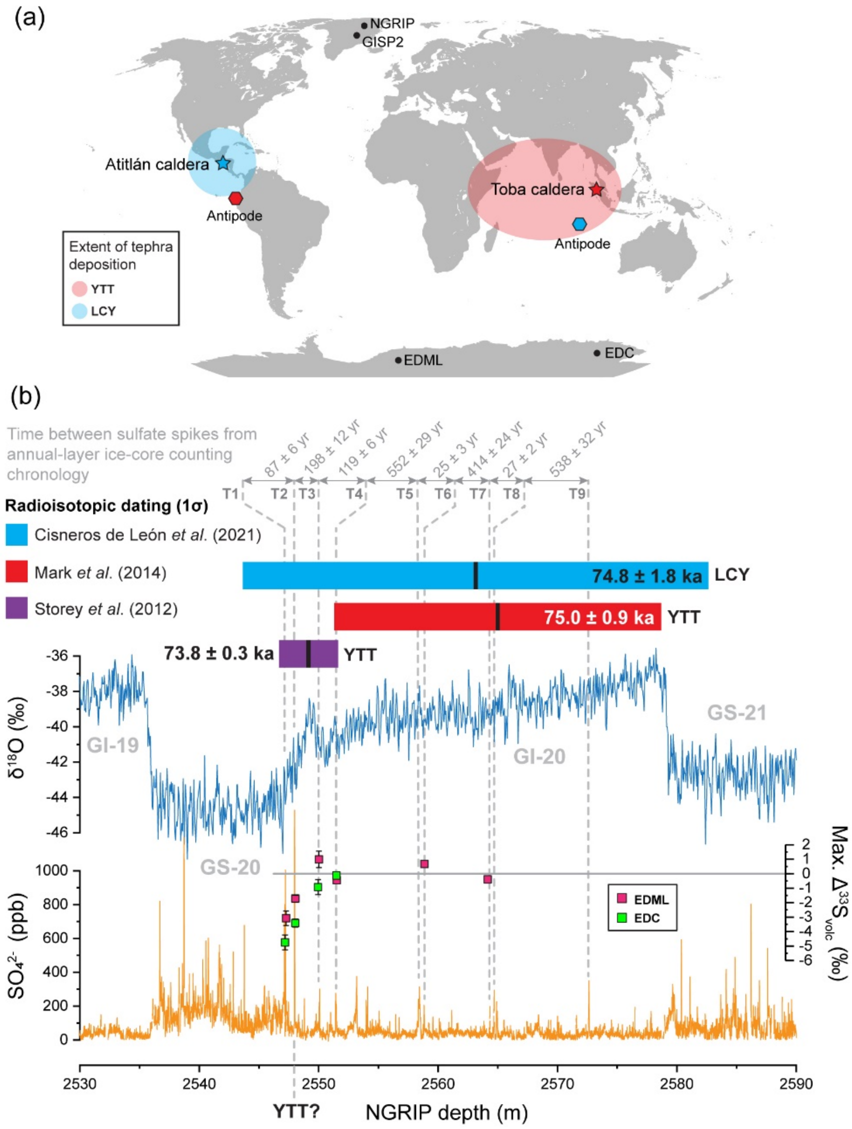

Figure 1. Spatial and geochronological information for YTT and LCY projected over climate and volcanic proxy signals from the northern and southern hemisphere ice core records. a) Map showing the location of Toba (Sumatra) and Atitlán calderas (Guatemala) as well as their respective antipodes (hexagons) along with their approximate tephra distribution. b) Synchronization of YTT and LCY radioisotopic ages and their 1σ uncertainty with the NGRIP oxygen isotope and sulfate concentration records around the Greenland Interstadial 20 (GI-20) and the Greenland Stadial (GS-20) as well as the sulfur isotopic compositions from the EPICA Dronning Maud Land (EDML, Antarctica), and EPICA dome C (EDC, Antarctica) ice core records (Crick et al., 2021). Dashed gray lines indicate the sulfate candidate anomalies for the

YTT supereruption in the NGRIP but also present in the Antarctic ice cores (Fig. S1). The relative timespan between sulfate anomalies is derived from ice-core annual counting layers from (Svensson et al., 2013). Sulfate anomalies between YTT candidates have been discarded as volcanic-derived signals by (Svensson et al., 2013), based on the lack of anomalies in other volcanic eruption proxies in the ice cores like electrical conductivity.

The new LCY age is strikingly close to that of YTT (overlapping within 1σ error), implying that in combination both eruptions would potentially have more impact on global climate than each eruption on its own (e.g., Toohey et al., 2016). Additionally, the close age concordance is intriguing from the perspective of teleconnections and causative linkages. Both supereruptions likely deposited relatively high amounts of sulfate on the ice sheets of the northern and southern hemispheres because of estimated high sulfur loads and tropical vent location (LCY = 523 ± 95 Mt (Brenna et al., 2020); YTT = 1,700–3,500 Mt (Costa et al., 2014)); though significant uncertainties on the validity of these estimations exists.

Timespan between YTT and LCY

Assuming that the YTT and LCY eruptions are represented by two of the nine sulfate spike candidates within the YTT eruption window, a relative time difference between the two supereruptions can be estimated by counting the ice-deposition annual layers (Svensson et al., 2013) (Fig. 1b). The estimated time window ranges from a maximum of *ca*. 2,000 yr (T1 to T9 spikes) and a minimum of *ca*. 25 yr (T5 to T6 spikes). We note that sulfate spikes (T1–T4) show large-magnitude sulfur mass-independent fractionation (S-MIF) isotopic signatures (Fig. 1b)(Crick et al., 2021), which are indicative for large eruptions from tropical locations whose plumes reached altitudes at or above the ozone layer in the stratosphere. If only the spikes associated with S-MIF are considered the potential maximum and minimum timespan between YTT and LCY could be further constrained to *ca*. 400 and 87 yr, respectively; orders of magnitude shorter than the estimated recurrence interval of supereruptions.

This close temporal correspondence between YTT and LCY (87–400 yr) is extraordinary given that individual supereruptions are extremely rare events in nature. If synchronous supereruptions are indeed anomalous events, the temporal proximity of YTT and LCY raises the question of whether there is a causal relationship between these two geologically concurrent events and if both could have resulted from a third underlying process? The location of Atitlán caldera being nearly antipodal to that of Toba caldera is also highly intriguing (Fig. 1a, ~2,200 km between the Atitlán caldera and the antipodal location of the Toba caldera), as is the almost identical zircon crystallization record from both magmatic systems (Fig. 2).

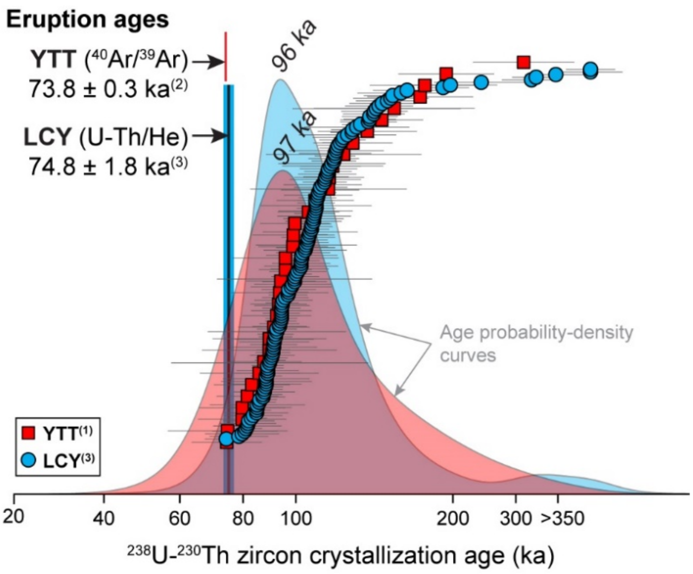

Fig. 2. Ranked order plot and probability-density curves for YTT and LCY zircon rim crystallization ages. Vertical bars represent radioisotopic ages for YTT and LCY eruptions, with colored-bar thicknesses representing corresponding 1σ uncertainty. Data from [1](Mucek et al., 2017), [2](Storey et al., 2012), and [3](Cisneros de León et al., 2021).

Supereruption clustering and statistical analysis

Although synchronous large eruptions have been suggested before for the Altiplano Puna Volcanic Complex of the Andes and the Taupo Volcanic Zone of New Zealand (de Silva et al., 2006; Gravley et al., 2007), these are from coeval regional magmatic systems that reasonably could be expected to be linked because of their spatial proximity and thermomechanical connectivity. At least in the Altiplano Puna Volcanic Complex, any assessment of true synchroneity is obscured by the limited resolution of the radioisotopic techniques. Other potential examples of synchroneity on a global scale may be represented by the Huckleberry Ridge Tuff (HRT) in the USA (2.0794 ± 0.0046 Ma)(Rivera et al., 2014) and Cerro Galán Ignimbrite (CGI) in Chile (2.08 ± 0.02 Ma)(Kay et al., 2011), but these lack the age precision to accurately constrain relative ages on a sub-kyr scale. They also lack the near antipodal positioning that stands out as a unique and compelling feature of the YTT-LCY connection (Fig. 3).

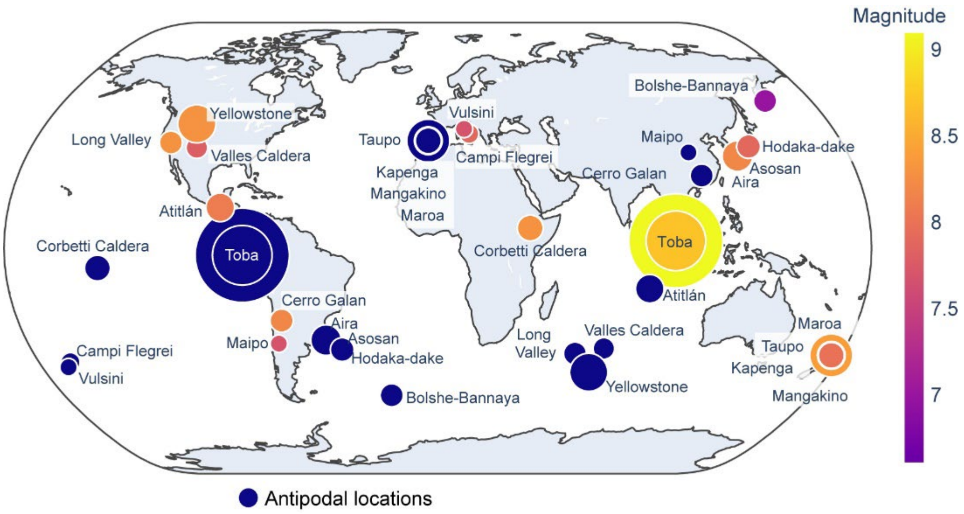

Fig. 3. Large volcanic eruptions (> 400 km^3) from the LaMEVE database over the last 2.1 Myr. Eruption magnitudes are represented by the size and color of the symbol. The antipodal location for each eruption is shown as blue circles. It is noteworthy that the main potentially antipodal relationship between two supervolcano eruptions also close in time is the YTT and LCY eruption pair. Note that Toba has sourced two Quaternary supereruptions, with YTT represented by the larger circle (id. Taupo).

We evaluate whether the temporal clustering of large eruptions is purely random using the timing of >400 km^3 bulk volume (>M7) Quaternary eruptions (LaMEVE)(Crosweller et al., 2012) that produced well-preserved deposits in the geological record. A relatively lower bulk volume than supereruptions was chosen to increase the sample size number (n = 28) for statistical analysis in order to avoid bias in the statistical analysis from having two coeval supereruptions (LCY and YTT) out of 13 in the past *ca*. 2 Myr (~10%). Additionally, this threshold ensures that our analysis is comparable to the global eruption frequency analysis for the largest VEI bin (VEI 7.5 and above) in Papale (2018). To assess any temporal eruption clustering in the geological record spanning the last *ca*. 2 Myr we calculated the coefficient of variation value (CV: the ratio of the standard deviation and the mean value for the time between two successive volcanic eruptions) for the reported eruption record (n = 28). Given the potential statistical bias from a small sampling number (n = 28), we used a Monte Carlo simulation (for details see Methods) to generate 50,000 different possible synthetic eruption histories after the reported eruption record and their 1σ uncertainties. The resulting median value of the CV for the reported eruption record distribution is ~1.035, whereas the median value of the mean time between eruptions is 76.28 kyr (28 eruptions in 2.054 Myr). Using the CV values obtained from the synthetic sequences of n equal to that of the reported Quaternary large eruptions (n = 28), we find that our >400 km^3 bulk volume LaMEVE distribution lies within the 5–95th percentile for a random distribution (inset Fig. 4). Thus, LaMEVE dataset as a whole does not display any significant non-randomness/clustering at the 95% confidence limit. This conclusion is further supported by the clear difference in the CV value between the LaMEVE dataset and synthetic eruption histories with either periodically spaced eruptions or close eruption pairs (~ 5% of the average time between eruption groups, Fig. S2). We would note that some of the statistical properties of the LaMEVE dataset are not fully consistent with a purely random (or Poisson) eruption history. Specifically, the most likely value for the median temporal gap between individual eruptions does not closely match the expectations for random eruption histories (Fig.

S3). However, based on our analysis of a variety of synthetic eruption histories (e.g., random, periodic, clustered, Fig. S4) and their differences concerning the median parameter, we posit that the LaMEVE dataset is likely a mostly random eruptive history with only a few eruption pairs (potentially YTT-LCY and HRT-CGI).

Finally, we estimate the occurrence of two supereruptions within a time range from 80 to 400 yr in a random eruptive history. Among 50,000 synthetic histories with random spacing between eruptions and volumes sampled from our LaMEVE dataset, we find that only 1.73% of the synthetic histories have an eruption pair that matches the YTT-LCY characteristics (Inset Fig. 4). The probability is still less than 2% even if we use a homogeneous Poisson process (e.g., Papale, 2018) as the model for eruption temporal distribution instead of a random distribution. Moreover, even if we assume that the LaMEVE database is only complete for the last 100 kyr as suggested by Rougier et al. (2018) (6 eruptions with >400 km^3 in last 100 kyr, recurrence time of *ca*. 17 kyr), there is still only a 4.2% probability of a YTT-LCY type eruption pair (Fig. S6). Thus, the statistical likelihood for two closely spaced supereruptions is small. This probability decreases further to only 0.086% when considering only synthetic eruption pairs at a comparable spatial distribution to the near antipodal nature of the Toba and Atitlán source calderas (Fig. S7) as shown in Fig. 3. Therefore, this spatial relationship between Atitlán and Toba is unique amongst any other large eruptions (Fig. 3 with >400 bulk volume eruptions), especially the M8 eruptions.

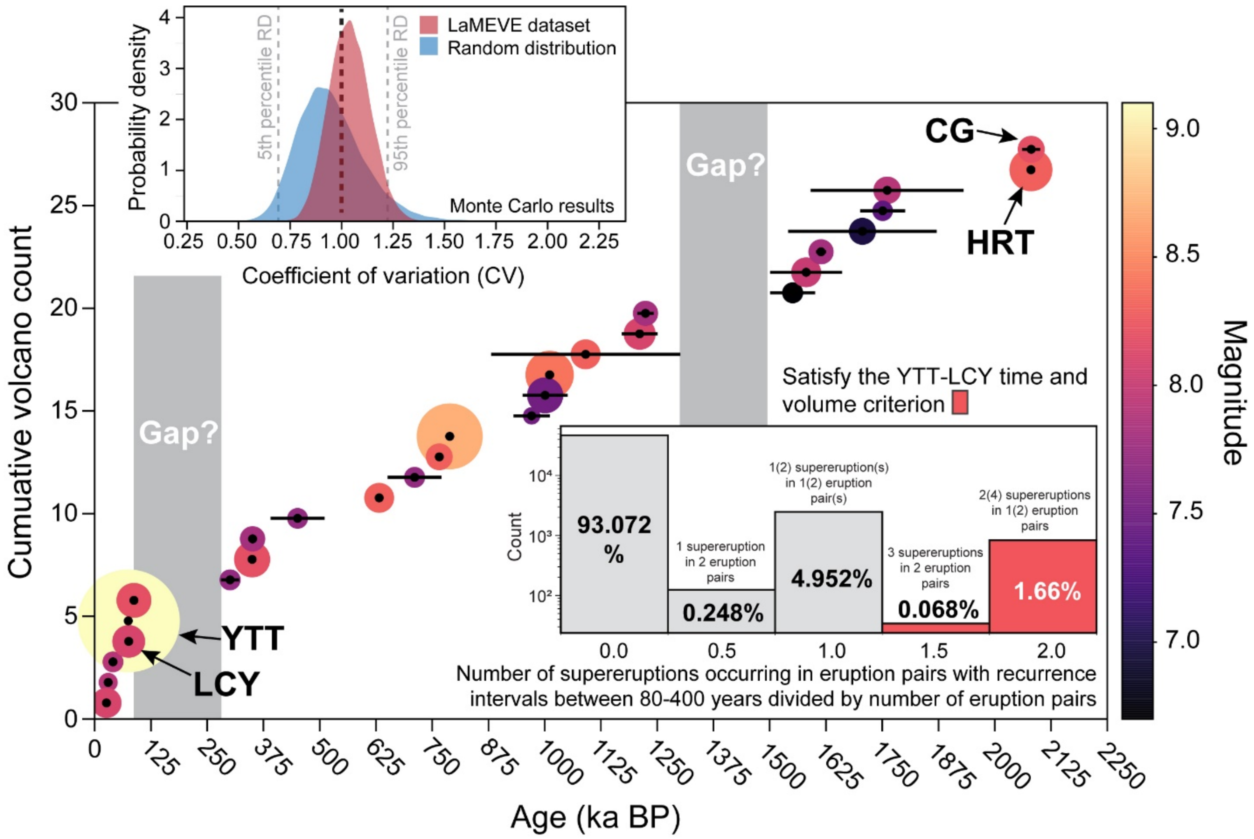

Figure 4. Cumulative number of eruptions (>400 km^3) through the last *ca*. 2.2 Myr from the LaMEVE database. The color and size of the symbols are representing the magnitude of the eruptions. Black bars through symbols are 1σ age uncertainties. The upper inset plot shows the probability density curves for the coefficient of variation (CV) values from both the reported eruption dataset from LaMEVE and that of 50,000 synthetic eruptive histories generated by a Monte Carlo algorithm. Values of CV >1 indicate clustering of eruptions and CV <1 periodic eruptions. The lower inset histogram shows the number of eruption histories (among 50,000 synthetic eruptions histories assuming that eruptions are randomly distributed) that contain paired eruptions within 80-400 years and at least one supereruption (>1000 km^3) divided by the number of eruption pairs. A paired supereruption with YTT-LCY characteristics would be represented by '1.5' or '2.0' (either 1 or 2 eruption pairs) on the x-axis. On the other hand, if only one of the two closely spaced eruptions is a supereruption, it would be represented by the '0.5' or '1' (either 1 or 2 eruption pairs) bin in the x-axis. The numbers on each histogram show the percentage probability of being in that bin based on the synthetic eruptive histories.

Physical processes for supereruption initiation

Given the unlikely nature of a randomly synchronous eruption between YTT and LCY, it is reasonable to consider if there could be a causal relationship between them. The near-antipodal positions of the Toba caldera in Sumatra and the Atitlán caldera in Guatemala may be key. Geological effects including extensive crustal fracturing and surface disruption have been reported in antipodal locations after major meteorite impacts on Mercury and the Moon resulting from spherical focusing of impact-generated seismic energy (Watts et al., 1991). On Earth, antipodal effects from meteorite impacts have been potentially associated with the triggering or enhancing of volcanic activity (Meschede et al., 2011; Richards et al., 2015). Large magnitude tectonically generated earthquakes have also been associated with antipodal seismic focusing (O'Malley et al., 2018). Nonetheless, triggering of one supereruption by another from the seismic moment released, especially lying at the opposite side of the globe, is yet an undocumented phenomenon and difficult to quantify as instrumental data of the elastic energy associated with supereruptions are non-existent (Gudmundsson, 2016). This notwithstanding, we note that an estimate for the total elastic energy released during the Toba supereruption is in the order of 10^{19} [J] (Gudmundsson, 2016), which is in the same order of magnitude as the largest instrumentally recorded earthquake, the M9.5 Chile (Valdivia) earthquake. As a comparison, the energy delivered by a meteorite impact like the Chicxulub event is estimated in the order of $\sim 10^{23}$ [J] (Boslough et al., 1996), which translates into seismic energy of $\sim 10^{18}$–10^{20} [J] after conversion into seismic efficiency (Shishkin, 2007). Although the rate of elastic energy released by the YTT supereruption is likely lower than a M9.5 earthquake or a large impact (due to much longer eruption duration), the total energy released is similar and may thus have similar effects on distal magmatic systems. The potential causal relationship between seismic energy and triggering or initiating of volcanic eruptions remains poorly constrained. It has been documented for only 0.4% of historical eruptions (Manga and Brodsky, 2006; Sawi and Manga, 2018) though this probability may increase to 10% when considering a 2 yr window between a leading large earthquake and a subsequent explosive eruption (Sawi and Manga, 2018). Causal effects are further supported by a temporal link between large magnitude earthquakes and volcanic activity at a global scale that has been proposed for the M9.1 Sumatra earthquake (Hill-Butler et al., 2020). Seismic activity has also been suggested as a potential trigger or initiation mechanism of supereruptions from perched magma reservoirs (Davis et al., 2007; Gregg et al., 2015). The dynamic stresses induced by passing seismic waves have been linked to the onset of different magmatic processes affecting the host-rock, magma chamber, or associated hydrothermal system (Seropian et al., 2021). The associated changes in magma overpressure, hydrothermal fluid pressure, and crustal and magmatic mush permeability can ultimately lead to an eruption (Davis et al., 2007; Richards et al., 2015; Seropian et al., 2021).

Large supereruption-feeding magma systems can remain petrologically buffered and thermomechanically primed at a critical threshold for extended periods of time (Caricchi and Blundy, 2015; Gregg et al., 2012). This pre-eruptive tipping point is most likely to be breached if roof instability can be initiated externally (Gregg et al., 2012). If YTT preceded the LCY and produced focused seismicity leading to a perturbation in the stress field of the crust below Atitlán caldera or in the roof of the magma reservoir, an eruption may be initiated and triggered if the magma was perched at the pre-eruptive tipping point. Long residence in a melt-present buffered state for both the YTT and LCY supervolcanic magmatic systems is suggested by protracted zircon crystallization records (Cisneros de León et al., 2021; Mucek et al., 2017; Reid and Vazquez, 2017). Notably, both LCY and YTT exhibit strikingly similar thermochemical histories for their corresponding magma reservoirs based on the crystallization of zircon and its sensitivity to changes in magma chemistry and temperature (Fig. 2). Magma accumulation timescales inferred from zircon rim crystallization ages of YTT and LCY are on the order of tens of thousands of years prior to the supereruption, with a remarkably coincident maximum at *ca*. 96 ka (Fig. 2). This suggests that the main phase of silicic magma differentiation and assembly of a melt-dominated magma body for YTT and LCY likely occurred within a similar time window of *ca*. 20 kyr before the eruption. Thus, zircon indicates an ongoing evolution of the Atitlán caldera magma reservoir towards a critical state similar to that experienced by YTT. In this scenario, we speculate that the passage of large period Rayleigh seismic waves through a crystal-mush-dominated reservoir may have affected the system's stability ultimately culminating in a supereruption on a decadal-century scale. Some potential physical processes include dynamic stresses due to passing seismic waves that induced pore pressure variations modifying the permeability structure of the crystalline matrix (Holtzman et al., 2003), and/or liquefaction of the crystalline mush (Sumita and Manga, 2008). Both of these processes (and similar visco-elastic two-phase instabilities in a magmatic mush) would promote new migration pathways for magma to ascend and increase local stresses in the magma reservoir ultimately leading to the eruption.

One natural expectation from our model is that the YTT event also primed smaller volcanic systems. However, given their smaller scale, these smaller eruptions are likely poorly preserved in the geologic record and/or remained unstudied. An exception could be the Arce tephra erupted from Coatepeque caldera in El Salvador, which produced two large silicic eruptions separated only by a couple of hundreds of years (~26 and 41 km^3)(Kutterolf et al., 2019) and whose age of 72 ± 2 ka (Rose et al., 1999) overlaps that of YTT and LCY.

Resolving whether the time-space relationship between YTT and LCY was not purely random but influenced by external factors would critically benefit from refining the absolute dating for both supereruptions (and other close supereruption pairs), preferentially by applying the same geochronological method. This also holds for assessing the climatic consequences of such paired supereruptions. The ultimate resolution for the time lapse between YTT and LCY could come from the identification of volcanic glass shards from both supereruptions within the ice-core layers. We deem such an endeavor promising because glass compositions from YTT and

LCY tephra are unambiguously distinct in trace element abundances (Fig. S7). No tangible evidence exists for a large extraterrestrial impact contemporaneous to the YTT-LCY eruption pair, but because of the low probability of random coincidence of the YTT-LCY supereruptions, such a "triple-whammy" scenario cannot be dismissed.

References

Abbott, P. M., Davies, S. M., Steffensen, J. P., Pearce, N. J., Bigler, M., Johnsen, S. J., Seierstad, I. K., Svensson, A., and Wastegård, S., 2012, A detailed framework of Marine Isotope Stages 4 and 5 volcanic events recorded in two Greenland ice-cores: Quaternary Science Reviews, v. 36, p. 59-77.

Ambrose, S. H., 1998, Late Pleistocene human population bottlenecks, volcanic winter, and differentiation of modern humans: Journal of Human Evolution, v. 34, no. 6, p. 623-651.

Bland, P. A., 2005, The impact rate on Earth: Philosophical Transactions of the Royal Society A: Mathematical, Physical and Engineering Sciences, v. 363, no. 1837, p. 2793-2810.

Boslough, M., Chael, E., Trucano, T., Crawford, D., and Campbell, D., 1996, Axial focusing of impact energy in the Earth's interior: A possible link to flood basalts and hotspots: Geological Society of America Special Papers, v. 307, p. 541-550.

Brenna, H., Kutterolf, S., Mills, M. J., and Krüger, K., 2020, The potential impacts of a sulfur- and halogen-rich supereruption such as Los Chocoyos on the atmosphere and climate: Atmos. Chem. Phys., v. 20, no. 11, p. 6521-6539.

Brenna, H., Kutterolf, S., Mills, M. J., Niemeier, U., Timmreck, C., and Krüger, K., 2021, Decadal Disruption of the QBO by Tropical Volcanic Supereruptions: Geophysical Research Letters, v. 48, no. 5, p. e2020GL089687.

Brown, S. K., Crosweller, H. S., Sparks, R. S. J., Cottrell, E., Deligne, N. I., Guerrero, N. O., Hobbs, L., Kiyosugi, K., Loughlin, S. C., and Siebert, L., 2014, Characterisation of the Quaternary eruption record: analysis of the Large Magnitude Explosive Volcanic Eruptions (LaMEVE) database: Journal of Applied Volcanology, v. 3, no. 1, p. 1-22.

Caricchi, L., and Blundy, J., 2015, The temporal evolution of chemical and physical properties of magmatic systems: Geological Society, London, Special Publications, v. 422.

Cisneros de León, A., Schindlbeck-Belo, J. C., Kutterolf, S., Danišík, M., Schmitt, A. K., Freundt, A., Pérez, W., Harvey, J. C., Wang, K. L., and Lee, H. Y., 2021, A history of violence: magma incubation, timing and tephra distribution of the Los Chocoyos supereruption (Atitlán Caldera, Guatemala): Journal of Quaternary Science, v. 36, no. 2, p. 169-179.

Costa, A., Smith, V. C., Macedonio, G., and Matthews, N. E., 2014, The magnitude and impact of the Youngest Toba Tuff super-eruption: Frontiers in Earth Science, v. 2, p. 16.

Crick, L., Burke, A., Hutchison, W., Kohno, M., Moore, K. A., Savarino, J., Doyle, E. A., Mahony, S., Kipfstuhl, S., Rae, J. W. B., Steele, R. C. J., Sparks, R. S. J., and Wolff, E. W., 2021, New insights into the ~74 ka Toba eruption from sulfur isotopes of polar ice cores: Clim. Past Discuss., v. 2021, p. 1-28.

Crosweller, H. S., Arora, B., Brown, S. K., Cottrell, E., Deligne, N. I., Guerrero, N. O., Hobbs, L., Kiyosugi, K., Loughlin, S. C., and Lowndes, J., 2012, Global database on large magnitude explosive volcanic eruptions (LaMEVE): Journal of Applied Volcanology, v. 1, no. 1, p. 1-13.

Davis, M., Koenders, M., and Petford, N., 2007, Vibro-agitation of chambered magma: Journal of Volcanology and Geothermal Research, v. 167, no. 1-4, p. 24-36.

de Silva, S., Zandt, G., Trumbull, R., Viramonte, J. G., Salas, G., and Jiménez, N., 2006, Large ignimbrite eruptions and volcano-tectonic depressions in the Central Andes: a thermomechanical perspective: Geological Society, London, Special Publications, v. 269, no. 1, p. 47-63.

Deligne, N. I., Sparks, R. S. J., and Brown, S. K., 2017, Report on potential sampling biases in the LaMEVE database of global volcanism: Journal of Applied Volcanology, v. 6, no. 1, p. 1-5.

Drexler, J. W., Rose, W. I., Sparks, R., and Ledbetter, M., 1980, The Los Chocoyos Ash, Guatemala: a major stratigraphic marker in Middle America and in three ocean basins: Quaternary Research, v. 13, no. 3, p. 327-345.

Gravley, D., Wilson, C., Leonard, G., and Cole, J., 2007, Double trouble: Paired ignimbrite eruptions and collateral subsidence in the Taupo Volcanic Zone, New Zealand: Geological Society of America Bulletin, v. 119, no. 1-2, p. 18-30.

Gregg, P., De Silva, S., Grosfils, E., and Parmigiani, J., 2012, Catastrophic caldera-forming eruptions: Thermomechanics and implications for eruption triggering and maximum caldera dimensions on Earth: Journal of Volcanology and Geothermal Research, v. 241, p. 1-12.

Gregg, P. M., Grosfils, E. B., and de Silva, S. L., 2015, Catastrophic caldera-forming eruptions II: The subordinate role of magma buoyancy as an eruption trigger: Journal of Volcanology and Geothermal Research, v. 305, p. 100-113.

Gudmundsson, A., 2016, The mechanics of large volcanic eruptions: Earth-science reviews, v. 163, p. 72-93.

Guttorp, P., and Thompson, M. L., 1991, Estimating second-order parameters of volcanicity from historical data: Journal of the American Statistical Association, v. 86, no. 415, p. 578-583.

Hill-Butler, C., Blackett, M., Wright, R., and Trodd, N., 2020, The co-incidence of earthquakes and volcanoes: assessing global volcanic radiant flux responses to earthquakes in the 21st century: Journal of Volcanology and Geothermal Research, v. 393, p. 106770.

Holtzman, B., Groebner, N., Zimmerman, M., Ginsberg, S., and Kohlstedt, D., 2003, Stress-driven melt segregation in partially molten rocks: Geochemistry, Geophysics, Geosystems, v. 4, no. 5.

Hooker, J., Laubach, S., and Marrett, R., 2018, Microfracture spacing distributions and the evolution of fracture patterns in sandstones: Journal of Structural Geology, v. 108, p. 66-79.

Kay, S. M., Coira, B., Wörner, G., Kay, R. W., and Singer, B. S., 2011, Geochemical, isotopic and single crystal 40 Ar/39 Ar age constraints on the evolution of the Cerro Galán ignimbrites: Bulletin of Volcanology, v. 73, no. 10, p. 1487-1511.

Kutterolf, S., Schindlbeck- Belo, J. C., Rohr, I., Rademacher, M., Cisneros de León, A., Eisele, S., Freundt, A., Hernandez, W., and Wang, K. L., 2019, The Arce Tephra: Two subsequent paroxysmal Plinian eruptions from Coatepeque Caldera (El Salvador): Journal of Volcanology and Geothermal Research, p. 106673.

Manga, M., and Brodsky, E., 2006, Seismic triggering of eruptions in the far field: Volcanoes and geysers: Annu. Rev. Earth Planet. Sci, v. 34, p. 263-291.

Mark, D. F., Petraglia, M., Smith, V. C., Morgan, L. E., Barfod, D. N., Ellis, B. S., Pearce, N. J., Pal, J., and Korisettar, R., 2014, A high-precision 40Ar/39Ar age for the Young Toba Tuff and dating of ultra-distal tephra: Forcing of Quaternary climate and implications for hominin occupation of India: Quaternary Geochronology, v. 21, p. 90-103.

Meschede, M. A., Myhrvold, C. L., and Tromp, J., 2011, Antipodal focusing of seismic waves due to large meteorite impacts on Earth: Geophysical Journal International, v. 187, no. 1, p. 529-537.

Miller, C. F., and Wark, D. A., 2008, Supervolcanoes and their explosive supereruptions: Elements, v. 4, no. 1, p. 11-15.

Mucek, A. E., Danišík, M., de Silva, S. L., Schmitt, A. K., Pratomo, I., and Coble, M. A., 2017, Post-supereruption recovery at Toba Caldera: Nature Communications, v. 8, no. 1, p. 15248.

O'Malley, R. T., Mondal, D., Goldfinger, C., and Behrenfeld, M. J., 2018, Evidence of systematic triggering at teleseismic distances following large earthquakes: Scientific reports, v. 8, no. 1, p. 1-12.

Oppenheimer, C., 2002, Limited global change due to the largest known Quaternary eruption, Toba≈ 74 kyr BP?: Quaternary Science Reviews, v. 21, no. 14-15, p. 1593-1609.

Osipov, S., Stenchikov, G., Tsigaridis, K., LeGrande, A. N., Bauer, S. E., Fnais, M., and Lelieveld, J., 2021, The Toba supervolcano eruption caused severe tropical stratospheric ozone depletion: Communications Earth & Environment, v. 2, no. 1, p. 1-7.

Papale, P., 2018, Global time-size distribution of volcanic eruptions on Earth: Scientific reports, v. 8, no. 1, p. 1-11.

Pearce, N. J., Westgate, J. A., Gualda, G. A., Gatti, E., and Muhammad, R. F., 2020, Tephra glass chemistry provides storage and discharge details of five magma reservoirs which fed the 75 ka Youngest Toba Tuff eruption, northern Sumatra: Journal of Quaternary Science, v. 35, no. 1-2, p. 256-271.

Pyle, D. M., 2015, Sizes of volcanic eruptions, The encyclopedia of volcanoes, Elsevier, p. 257-264.

Rampino, M. R., 2002, Supereruptions as a threat to civilizations on Earth-like planets: Icarus, v. 156, no. 2, p. 562-569.

Rampino, M. R., and Self, S., 1992, Volcanic winter and accelerated glaciation following the Toba super-eruption: Nature, v. 359, no. 6390, p. 50-52.

Reid, M. R., and Vazquez, J. A., 2017, Fitful and protracted magma assembly leading to a giant eruption, Youngest Toba Tuff, Indonesia: Geochemistry, Geophysics, Geosystems, v. 18, no. 1, p. 156-177.

Richards, M. A., Alvarez, W., Self, S., Karlstrom, L., Renne, P. R., Manga, M., Sprain, C. J., Smit, J., Vanderkluysen, L., and Gibson, S. A., 2015, Triggering of the largest Deccan eruptions by the Chicxulub impact: Bulletin, v. 127, no. 11-12, p. 1507-1520.

Rivera, T. A., Schmitz, M. D., Crowley, J. L., and Storey, M., 2014, Rapid magma evolution constrained by zircon petrochronology and 40Ar/39Ar sanidine ages for the Huckleberry Ridge Tuff, Yellowstone, USA: Geology, v. 42, no. 8, p. 643-646.

Robock, A., Ammann, C. M., Oman, L., Shindell, D., Levis, S., and Stenchikov, G., 2009, Did the Toba volcanic eruption of~ 74 ka BP produce widespread glaciation?: Journal of Geophysical Research: Atmospheres, v. 114, no. D10.

Roche, O., Buesch, D. C., and Valentine, G. A., 2016, Slow-moving and far-travelled dense pyroclastic flows during the Peach Spring super-eruption: Nature communications, v. 7, p. 10890.

Rose, W. I., Conway, F. M., Pullinger, C. R., Deino, A., and McIntosh, W. C., 1999, An improved age framework for late Quaternary silicic eruptions in northern Central America: Bulletin of Volcanology, v. 61, no. 1-2, p. 106-120.

Rougier, J., Sparks, R. S. J., Cashman, K. V., and Brown, S. K., 2018, The global magnitude–frequency relationship for large explosive volcanic eruptions: Earth and Planetary Science Letters, v. 482, p. 621-629.

Sawi, T. M., and Manga, M., 2018, Revisiting short-term earthquake triggered volcanism: Bulletin of Volcanology, v. 80, no. 7, p. 1-9.

Self, S., 2015, Explosive super-eruptions and potential global impacts, Volcanic Hazards, Risks and Disasters, Elsevier, p. 399-418.

Seropian, G., Kennedy, B. M., Walter, T. R., Ichihara, M., and Jolly, A. D., 2021, A review framework of how earthquakes trigger volcanic eruptions: Nature Communications, v. 12, no. 1, p. 1-13.

Shishkin, N., 2007, Seismic efficiency of a contact explosion and a high-velocity impact: Journal of Applied Mechanics and Technical Physics, v. 48, no. 2, p. 145-152.

Storey, M., Roberts, R. G., and Saidin, M., 2012, Astronomically calibrated 40Ar/39Ar age for the Toba supereruption and global synchronization of late Quaternary records: Proceedings of the National Academy of Sciences, v. 109, no. 46, p. 18684-18688.

Sumita, I., and Manga, M., 2008, Suspension rheology under oscillatory shear and its geophysical implications: Earth and Planetary Science Letters, v. 269, no. 3-4, p. 468-477.

Svensson, A., Bigler, M., Blunier, T., Clausen, H. B., Dahl-Jensen, D., Fischer, H., Fujita, S., Goto-Azuma, K., Johnsen, S., and Kawamura, K., 2013, Direct linking of Greenland and Antarctic ice cores at the Toba eruption (74 ka BP): Climate of the Past, v. 9, no. 2, p. 749-766.

Toohey, M., Krüger, K., Sigl, M., Stordal, F., and Svensen, H., 2016, Climatic and societal impacts of a volcanic double event at the dawn of the Middle Ages: Climatic Change, v. 136, no. 3, p. 401-412.

Wang, T., Schofield, M., Bebbington, M., and Kiyosugi, K., 2020, Bayesian modelling of marked point processes with incomplete records: volcanic eruptions: Journal of the Royal Statistical Society: Series C (Applied Statistics), v. 69, no. 1, p. 109-130.

Watts, A. W., Greeley, R., and Melosh, H., 1991, The formation of terrains antipodal to major impacts: Icarus, v. 93, no. 1, p. 159-168.

Williams, M., 2012, The~ 73 ka Toba super-eruption and its impact: history of a debate: Quaternary International, v. 258, p. 19-29.

Acknowledgments

Funding: ACDL acknowledges funding support from the Deutsche Forschungsgemeinschaft (DFG) grants SCHM 2521/6-1 and KU2685/7-1; TM acknowledges funding support from the Crosby Postdoc Fellowship at MIT; SdeS acknowledges support from National Science Foundation grant EAR 1551187 for studies of the Toba caldera. **Author contributions:** Conceptualization ACdeL, TM, SdeS, SS, AKS, SK; Methodology: TM, ACdeL; Formal analysis: TM; Investigation: ACdeL, TM; Visualization: ACdeL, TM; Writing – original draft: ACdeL, TM; Writing – review & editing: ACdeL, TM, SdeS, SS, AKS, SK. **Competing interests:** The authors declare no competing interests. **Data and materials availability:** All

data used in this study are from previously published work, no new data was collected as part of this study. In the final manuscript, we will provide the Python notebook for analysis as supplementary material.

Supplementary Materials

Methods

To quantify the potential temporal clustering of large volcanic eruptions (>400 km^3 bulk volume) we used the Large Magnitude Explosive Volcanic Eruptions database (LaMEVE)(Crosweller et al., 2012). The LaMEVE database provides the best global compilation of aerial volcanic eruption ages and magnitudes during the Quaternary (Brown et al., 2014; Crosweller et al., 2012). We choose a large volume range cutoff (typically corresponding to magnitude (M) >7 eruptions or Volcanic Explosivity Index (VEI) 7–8 eruptions) since the largest eruptions are most likely to be recorded in the geologic record. This conclusion is further supported by the observation that the cumulative number of eruptions through time (Fig. 4, 28 eruptions total) has an approximately linear relationship in our dataset. Assuming the eruption rate is effectively time-invariant, strong decreases in the eruption recording probability back in time would show up as a convex non-linearity in this plot (Guttorp and Thompson, 1991; Rougier et al., 2018) and this is observed for less well preserved lower volume eruptions (Papale, 2018; Rougier et al., 2018). Nevertheless, there are some gaps in the LaMEVE eruption record (e.g., between 100–275 kyr, 1275–1500 kyr, Fig. 4) which may either be indicative of unrecorded eruptions (more likely though there is no clear relationship with glacial-interglacial periods) or some episodic tectonic process. An analysis of the database biases is beyond the scope of our analysis and we refer the reader to the original LaMEVE papers (Brown et al., 2014; Crosweller et al., 2012), 2014) and Deligne et al. (2017) for a detailed discussion. We choose a lower volume threshold of 400 km^3 to ensure that we have enough eruptions in the dataset to allow robust statistical analysis. Additionally, this threshold ensures that our dataset is very similar to the VEI-8 category dataset in Papale (2018) analysis of recurrence interval for large eruption dataset. We find that the main results of our analysis are not sensitive to the specific volume threshold and are valid as long as we are only considering large (typically a few hundred km^3 eruptions).

We assess any temporal eruption clustering using the coefficient of variation (CV): the ratio of the standard deviation and the mean time interval between two successive volcanic eruptions. The CV (also called: relative standard deviation) is a commonly used statistical measure for analyzing the clustering of discrete events in time (e.g., earthquakes) (Hooker et al., 2018). Typically, CV values are close to 1 for randomly distributed data, >1 for clustered eruptions, and <1 for eruptions with a constant inter-eruption recurrence time (Hooker et al., 2018). Since some volcanic eruptions in the LaMEVE have a significant age uncertainty, we use a Monte-Carlo method to generate 50,000 different possible eruption histories by sampling from the reported eruption ages and their 1σ uncertainties. Using these eruption histories, we calculated the CV value as well as the mean and median recurrence time between large eruptions (inset Fig. 4 and Fig. S2). The median value of the CV distribution is ~1.035, indicating an approximately random distribution. Similarly, the median value of the mean time between eruptions is 76.28 kyr which is close to the value expected for a random distribution (28 eruptions in 2.054 Ma) as well as the results from (Papale, 2018) for VEI 8 eruptions (*ca*. 78 kyr). Finally, although the median value of time between LaMEVE eruptions has a large spread between different possible eruptive histories (Fig. S3), the peak of the probability distribution is *ca*. 35 kyr.

Since our eruption catalog only has a small number of data points (N_{erupt} = 28 eruptions) which can bias statistical interpretations, we generate synthetic random eruption sequences with the same number of eruptions and total sequence duration as our catalog. Using the CV values from these synthetic sequences, we find the LaMEVE distribution lies within the 5–95th percentile values for the random distribution (inset Fig.4; Fig. S2). Thus, on the scale of the whole dataset, the LaMEVE >400 km^3 eruptions do not have any significant non-randomness at the 95%

confidence limit. This conclusion is further supported by the clear overlap between the mean time between eruptions for the synthetic random sequences and the LaMEVE data. However, there is a difference between probability density functions of the median time between eruptions and the synthetic histories. As discussed in more detail later, we interpret this observation to suggest that the LaMEVE dataset likely has a few eruption groups. Since our LaMEVE dataset includes the potential YTT-LCY and Huckleberry Ridge Tuff (HRT)-Cerro Galán Ignimbrite (CGI) pairs, this conclusion is not unexpected.

As a test to illustrate that our statistical analysis is robust and compare CV for clustered and periodic eruption scenarios, we generate 50,000 synthetic eruptive histories with either 2/3/4 clustered eruptions or with periodic eruptions. For the clustered eruption cases, we chose the maximum spacing between individual eruption clusters to be 5% (as well as 40% for the 2-cluster case, this is close to a random case) of the mean time between eruption clusters. Individual eruptive histories are generated by first sampling a random eruptive history with $N_{erupt}/2$; $N_{erupt}/3$; or $N_{erupt}/4$ eruptions and then adding the clustered eruption pairs with random spacing between 1 yr and the maximum spacing (e.g., 5% of the spacing between eruption clusters). For the periodic eruption histories, we set N_{erupt} eruption ages equally spaced over the LaMEVE dataset duration (~2.054 Ma) and assign a 1σ age uncertainty equal to 5% or 30% of the eruption spacing. Then, we generate synthetic histories with the same number of eruptions (N_{erup} = 28) as the LaMEVE dataset. As shown in Supplementary Fig. 2, the CV values for these eruptive histories are distinctive from the LaMEVE dataset with CV >1 for clustered eruptions and CV <1 for periodic eruptions as expected. Additionally, a random eruptive history with ~1000 eruptions has a CV ~1 as theoretically expected (Hooker et al., 2018). Among non-random histories, the closest match with the observed CV values is the 2-cluster case with maximum spacing between individual eruption clusters equal to 40% of the mean inter-cluster temporal spacing. We find the same qualitative result when comparing the median time between eruptions (Fig. S4) where the random and 2-cluster (with 40% variation) is the closest match to the observations. Since the presence of very closely spaced eruption clusters decreases the median time between eruptions (see Fig. S4), we posit that the most parsimonious explanation for the LaMEVE dataset is that it represents a combination of mostly randomly distributed eruptions along with a few closely spaced pairs (e.g., YTT-LCY, HRT-CGI). Given the significant uncertainties in eruption ages for many eruptions in the LaMEVE catalog as well as open questions regarding catalog completeness, it is challenging to presently make any stronger conclusions regarding eruption clustering of large volcanic eruptions.

Finally, we estimate how closely spaced two eruptions can be in a N_{erupt} (=28) random eruptive history. We also assign a bulk eruption volume to every volcanic eruption in each random eruptive history by randomly shuffling the volumes of the eruptions in our LaMEVE dataset. Thus, by construction, the probability density of eruption volumes in each synthetic history is the same as the observed dataset. We would note that herein we have assumed that there is no correlation between eruption volumes and when they erupt. Although this may not be exactly true in practice, this assumption provides a clear statistical end-member to compare against the observations. We use a similar methodology to assign a spatial location for each synthetic eruption by randomly shuffling the locations of our LaMEVE eruptions. Among the 50,000 synthetic histories, we find 2%, 10.15%, 16.392%, and 20% histories with a minimum time between two eruptions being < 80 years, 80–400, 400–1000, and 1000–2000 years, respectively (Fig. S5). However, if we also consider the volume of these eruption pairs, the joint probability of two eruptions spaced between 80 to 400 years and having ≥1000 km^3 volumes are much lower (Fig. 4). Finally, we can consider a constraint that a close-in-time (80-400 yr) supereruption pair must have a small distance (<3000 km) between the antipodal location of the first eruption in the pair and the location of the second eruption. This is motivated by the small similar distance between YTT-LCY (~2200 km). With this additional constraint, the total probability is even lower (Fig. S7).

In conclusion, for a randomly distributed eruption sequence, it is unlikely to observe close eruption pairs like Toba and LCY. As a final note, we acknowledge that our statistical results are weakly dependent on the choice of the underlying statistical model for eruption spacing (Papale, 2018; Rougier et al., 2018; Wang et al., 2020). For instance, a common model for eruption return times is the homogeneous Poisson process with exponential distribution of return times naturally leading to some long-time gaps (Papale, 2018). With this model, they find a very similar result for the mean recurrence time between eruptions (*ca*. 78 kyr) as our results as well as the probability of having a YTT-LCY eruption pair. It is noteworthy that Rougier et al. (2018), also using the LaMEVE database, but only for the last 100 kyr eruptions, find a much shorter (*ca*. 17 ka) recurrence time between M8 eruptions with their statistical model compared to other analysis. They argue for systematic biases in the volume estimates of very large explosive eruptions due to spatially widely distributed deposits for older eruptions. This illustrates that ultimately the accuracy of our conclusions is dependent on the veracity of the geologic constraints for large eruptions especially the accuracy of volume values reported in the LaMEVE database and the confidence in database completeness. To assess how a higher eruption recurrence rate (as argued by Rougier et al. (2018)) may affect our results, we repeated the statistical analysis with only eruptions in the last 100 kyr ($n = 6$ eruptions). Given the smaller number of eruptions, the statistical results for CV are less clear with a larger possible range from synthetic eruption histories. Nevertheless, CV from the 100 kyr LaMEVE dataset is consistent with random eruption distribution as a whole. Additionally, the likelihood of having two eruptions between 80 to 400 years and each having greater than 1000 km^3 volume is still less than 5% (Fig. S6).

Overall, our results are consistent with previous work in showing that presently, there is no strong evidence for eruption clustering for > 400 km^3 Bulk Volume eruptions in the LaMeVE database as a whole. Instead, the dataset is consistent with randomly distributed eruptions within only a few double eruption couplets. This result further highlights that the YTT-LCY eruption doublet is a unique circumstance.

Finally, we plotted published glass shards major and trace-element data for YTT and LCY (Cisneros de León et al., 2021; Pearce et al., 2020) in order to test whether both supereruptions can be easily discriminated if tephra was to be found in ice-core records (Fig. S8).

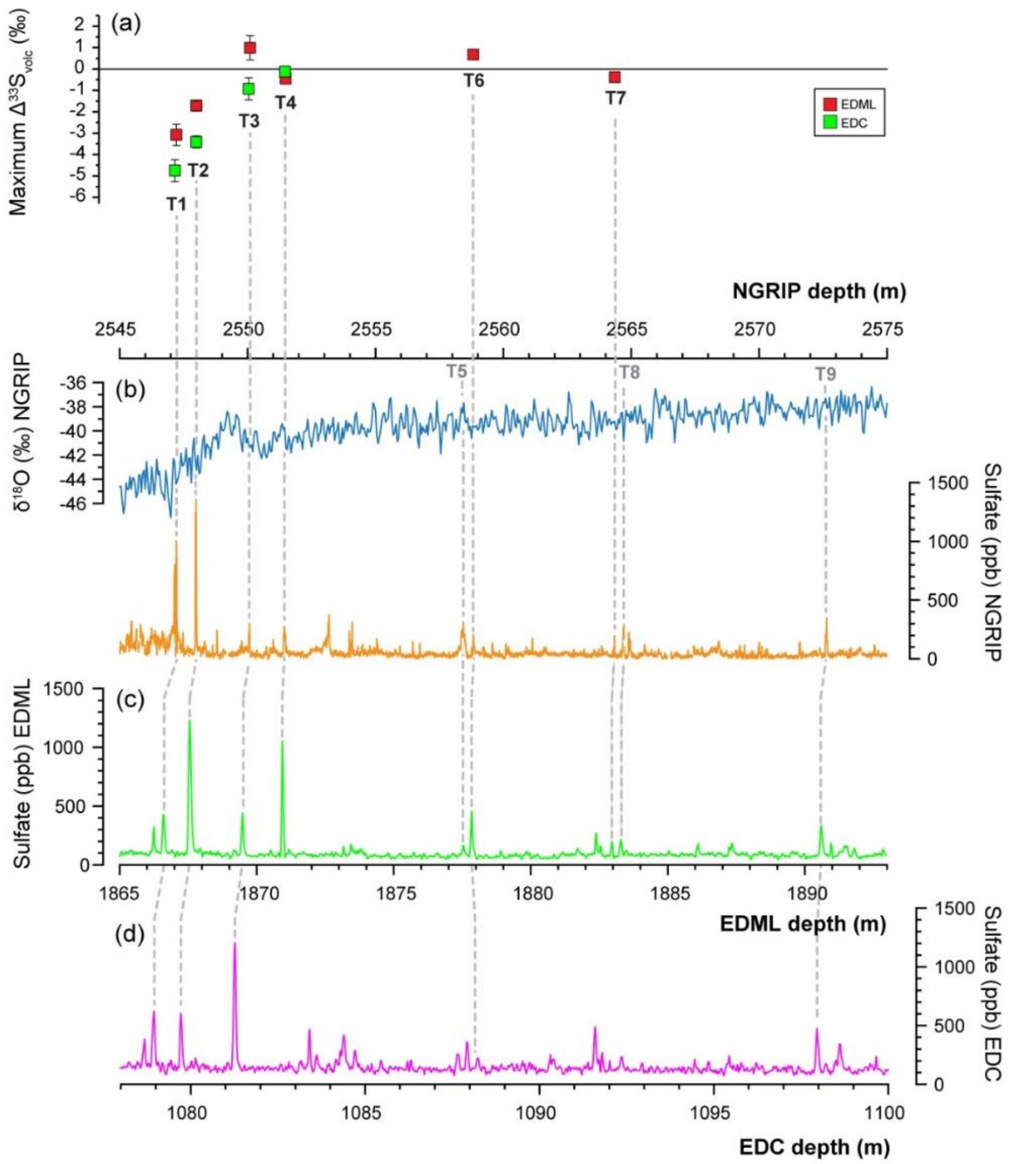

Fig. S1. Correlation of sulfur isotope compositions ($\Delta^{33}S$) from ice core layers containing the sulfate anomalies that are potentially associated with YTT and LCY with records of oxygen (NGRIP) and sulfate from the NGRIP, EPICA Dronning Maud Land (EDML, Antarctica), and

EPICA dome C (EDC, Antarctica) bipolar ice core records. Modified from (Crick et al., 2021) and (Svensson et al., 2013).

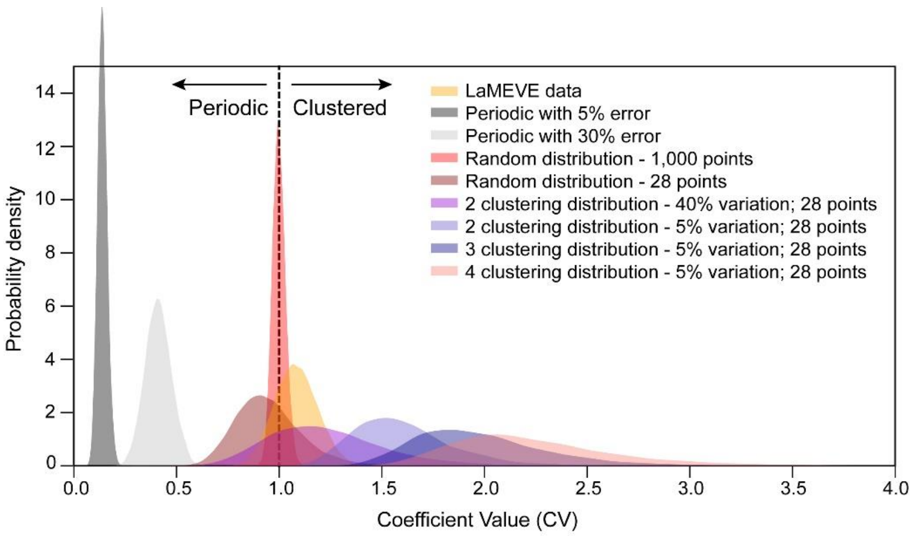

Fig. S2. Coefficient of variation (CV) Monte Carlo synthetic results. Analysis of the Coefficient of Variation for 50,000 synthetic eruptive histories with different statistical models - random, clustered, and periodic. We also plot the results from the LaMEVE dataset for comparison.

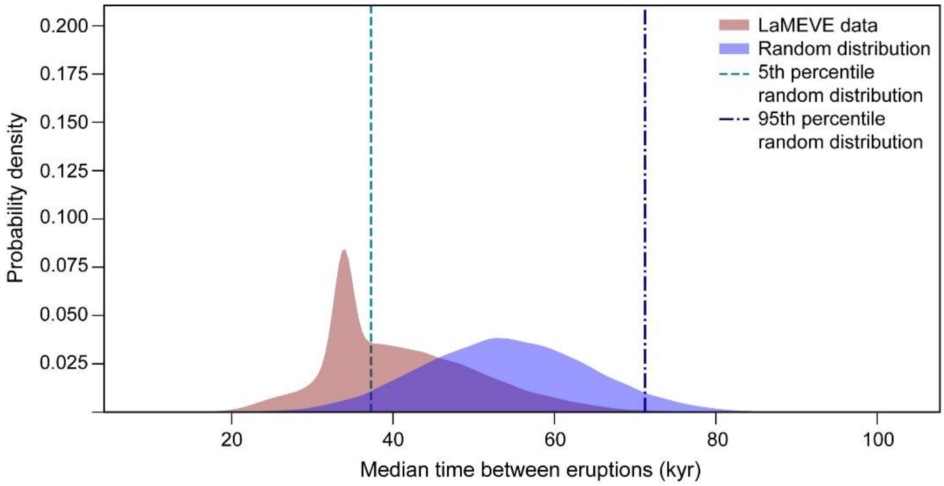

Fig. S3. Median time between eruptions (Monte Carlo results). Analysis of the Median value of the time between individual eruptions for the LaMEVE Dataset and 50,000 synthetic eruptive histories wherein the eruptions (28 eruptions, same as LaMEVE dataset) are randomly distributed in time.

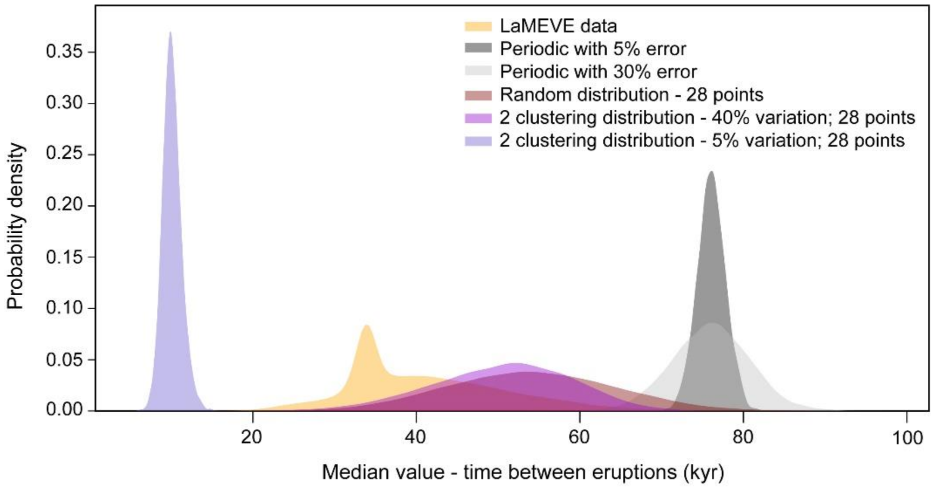

Fig. S4. Median value for time between eruptions. Analysis of the median value of the time between individual eruptions for 50,000 synthetic eruptive histories with different statistical models - random, clustered, and periodic. We also plot the results from the LaMEVE dataset for comparison.

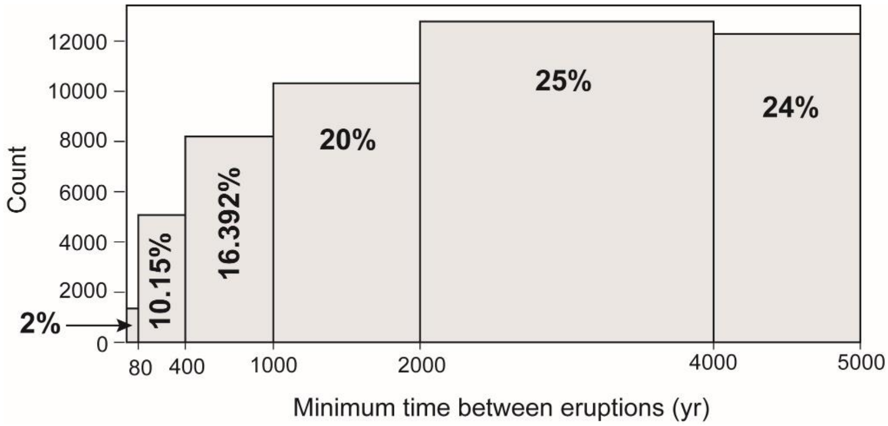

Fig. S5. Histogram of minimum time between subsequent eruptions for 50,000 synthetic eruptions histories assuming that eruptions are randomly distributed. The numbers on each histogram show the percentage probability of being in that bin based on the synthetic eruptive histories. We would note that here we are only considering the time between eruptions and not the volumes of each eruption which provides additional constraints on the likelihood of a large volume YTT-LCY pair.

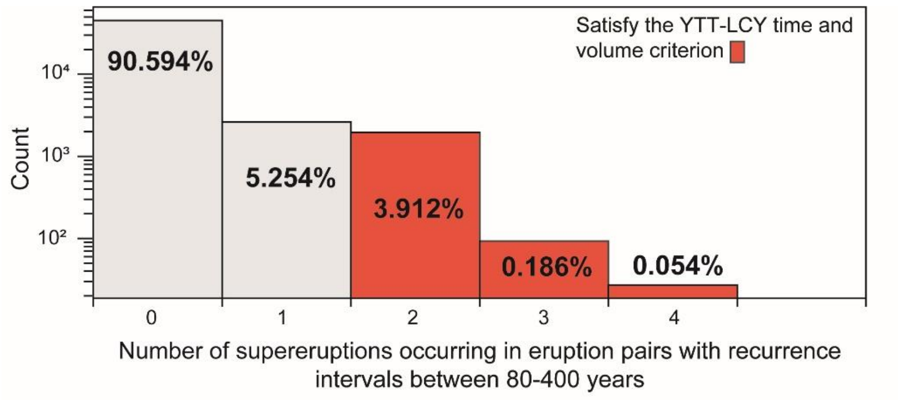

Fig. S6. Histogram showing how many eruption histories (among 50,000 synthetic eruptions histories assuming that eruptions are randomly distributed) have two eruptions within 80-400 years and volumes ≥1000 km^3 (supereruption). In contrast to Fig. 4, we only use the eruption frequency estimates from eruptions over the past 100 kyr. A supereruption pair like YTT-LCY would be represented by the '2' bin. On the other hand, if only one of the two closely spaced eruptions is a supereruption, it would be represented by the '1' bin. The numbers on each histogram show the percentage probability of being in that bin based on the synthetic eruptive histories.

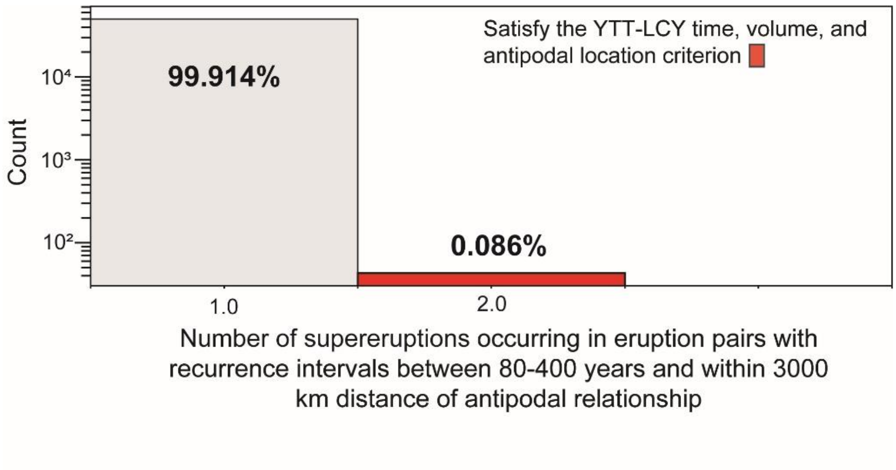

Fig. S7. Histogram showing number of eruption histories (among 50,000 synthetic eruptions histories assuming that eruptions are randomly distributed) that have two supereruptions within 80-400 years and a spatial relationship <3000 km distance between the antipodal location of the first eruption in the eruption pair and the second eruption's location. The numbers on each histogram show the percentage probability of being in that bin based on the synthetic eruptive histories.

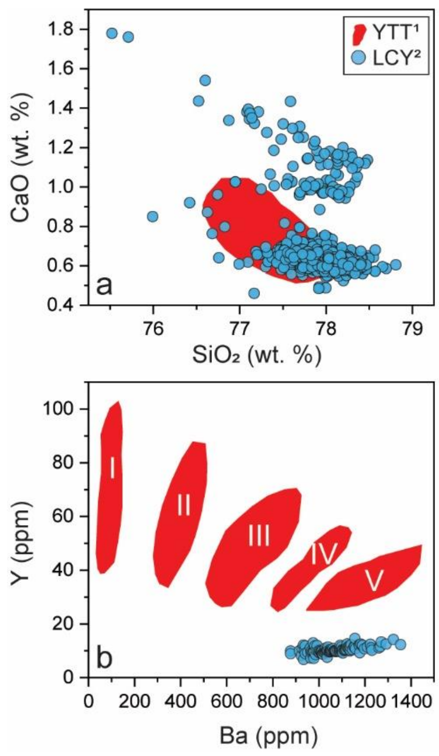

Fig. S8. Major and trace elements compositions for YTT and LCY glass shards. a) Major element compositions and b) Trace element compositions for YTT and LCY glass shards. YTT data from (Pearce et al., 2020) and LCY data from (Cisneros de León et al., 2021).